JOURNAL OF PROPULSION AND POWER
Vol. 15, No. 6, November–December 1999

Burning Rate of Solid Propellant Ingredients, Part 1: Pressure and Initial Temperature Effects

A. I. Atwood,* T. L. Boggs,† P. O. Curran,‡ T. P. Parr,§ and D. M. Hanson-Parr§
U.S. Naval Air Warfare Center, China Lake, California 93555
and
C. F. Price¶ and J. Wiknich**
Sverdrup, Inc., Ridgecrest, California 93555

Burning rate data are presented with respect to initial temperature and pressure for three compounds that are currently used in propellant and explosive formulations. The dependence of burning rate on initial temperature and pressure is presented for ammonium perchlorate (AP), HMX, and RDX. Data for ingredients being considered for advanced propellants, such as CL-20, ammonium dinitramide (ADN), and hydrazinium nitroformate (HNF) are also presented and compared to the more traditional compounds. These ingredients are all capable of self-deflagration, and their behavior often controls the behavior of the propellants in which they are the main ingredients.

Introduction

THE burning rate data presented in this paper represent the first part of a two-part presentation that was made at the International Workshop on Combustion Instability of Solid Propellants and Rocket Motors, June 1997, at the Politecnico di Milano, Milan, Italy. The burning rate temperature sensitivity data are being used to understand the mechanisms of intrinsic combustion stability with respect to propellant formulations. A thorough understanding of the burning rate temperature sensitivity is a key element in the analytical determination of the propellant combustion response when using such methods as the Zeldovich–Novozhilov analysis.[1]

Propellant burning rate pressure and temperature sensitivity are fundamental ballistic properties. They are vital in the evaluation of not only propellant performance but also in its hazards response. The linear burning rate is often described over a specific pressure range by the empirical relationship of $r_b = cp^n$. According to a commonly accepted but approximate view,[2] c is an empirical constant influenced by ambient temperature, and the exponent n, known as the pressure exponent, is independent of the temperature but describes the influence of pressure on burning rate. As n approaches 1, the burning rate is very sensitive to small changes in pressure. It can be seen that low values of n are desirable.

The dependence of burning rate on initial temperature is particularly important for missiles that encounter a wide range of temperatures in the course of their operation. An air-launched missile may be exposed to temperatures between 220 and 350 K. Obviously, the temperature dependence of the burning rate should be as low as possible so that the pressure and thrust is least affected by operation over a broad range of temperatures. The propellant burning rate temperature sensitivity is also important to hazards, because propellant is often at an elevated temperature when it ignites during these events.

Burning rate data for a number of energetic solid monopropellants have been collected over a number of years by several researchers at China Lake using various experimental measurement techniques.[3] Care has been taken to overlap the data of the different experimental techniques in such a way that a self-consistent burning rate data set for each material is available. The ability to predict the linear burning rate of a propellant as a function of initial pressure and temperature is a highly desirable goal, and the prediction of monopropellant deflagration is an initial step in this direction. The burning rate data presented in this paper serve as input into various modeling efforts currently in progress.[4,5]

Samples

Burning rate data are presented for the six monopropellants listed in Table 1. Several types of samples were used in making the burning rate measurements and are listed under the specific ingredient sections. The monopropellant samples included in some cases large, high-purity, single crystals, pressed pellets, and in one case, bulk powder. In the studies where more than one sample type was used, care was taken to overlap the test conditions so that the results were not biased by sample configuration. It should be noted that attempts to burn ammonium nitrate as a monopropellant have proven unsuccessful for the conditions tested to date.

Experiment

The burning rates presented were generated over the range of pressures from 0.24 to 345 MPa. Three separate experiments were required to achieve this range of pressures. Two of the experiments that provided the burning rate data from 0.24 to 55 MPa employed cinephotomicrography.[6] The pressures from 34.5 to 345 MPa were achieved using a closed bomb combustion technique.[7]

In the photocinemicrographic method, the propellant sample is pressurized in the combustion vessel to the desired test pressure, and a photograph of the sample regression due to combustion is made for analysis of the burning rate. A small enough sample is burned relative to the chamber volume to prevent any significant pressure contribution from the combusting gases. The burning propellant sample is photographed at 1× magnification at 400 frames per second using a Locam motion picture camera. A combination of two high-speed motion picture window bomb experiments were used for this study. A schematic of the standard window bomb is shown in Fig. 1. The 2500 W xenon lamp was used to illuminate the sample. The infrared filter prevents the heating of the sample by the lamp. A frame-by-frame analysis of the motion picture film is made with a Vanguard motion analyzer. Burning rate measurements of the propellant samples were made using the standard window bomb technique at pressures from 0.24 to 10.3 MPa at initial temperatures up to 423 K. The elevated initial temperatures were achieved

Received 7 February 1998; revision received 8 April 1999; accepted for publication 12 April 1999.

*Physical Scientist, Code 4T4310D, Research Department, Weapons Division.
†Head, Engineering Science Division, Code 4T4300D, Research Department, Weapons Division.
‡Engineering Technician, Code 4T4310D, Research Department, Weapons Division.
§Research Chemist, Code 4T4320D, Research Department, Weapons Division.
¶Scientist/Engineer, Systems Engineering/T&E Department.
**Senior Technical Staff, Systems Engineering/T&E Department.

Table 1 Solid monopropellants used in burning rate studies

Ingredient	Acronym
Ammonium perchlorate	AP
Ammonium dinitramide	ADN
Cyclotetramethylene tetranitramine	HMX
Cyclotrimethylene trinitramine	RDX
Hexanitrohexaazaisowurtzitane	CL-20
Hydrazinium nitroformate	HNF

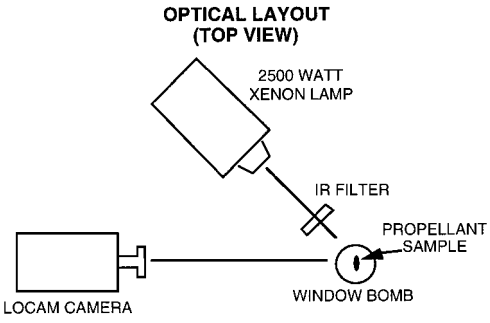

Fig. 1 Schematic of the standard window bomb.

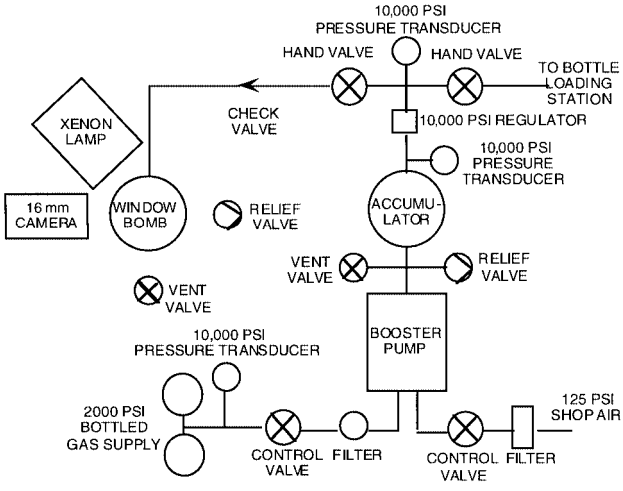

Fig. 2 Schematic of the high-pressure window bomb.

by preheating the combustion vessel, pressurizing gas, and sample. Propellant samples were tested in the standard window bomb at reduced temperature at pressures up to 6.2 MPa nitrogen using the Parr technique (see Ref. 8). In this method, a portion of the pressurizing nitrogen was cooled in a cold bath, and then it flowed through the sample mounting post and over the sample.

A high-pressure window bomb is used to evaluate the burning rates of the samples at pressures up to 55 MPa at ambient initial temperature only. A schematic of the high-pressure window bomb is shown in Fig. 2. This vessel primarily differs from the standard window bomb in that it has a heavier walled combustion chamber and smaller windows. Standard nitrogen pressure is increased using a Haskel booster pump. The accumulator is charged to the desired operating pressure to avoid rapid pressure fluctuations in the combustion vessel.

The accuracy of burning rate measurements using the photographic technique runs between 3 and 5%, but is dependent on the quality of the photograph and the inherent reproducibility of the sample. Temperatures are controlled to $\pm 1^{\circ}$C at the elevated temperatures and $\pm 3^{\circ}$C at the reduced temperatures. Ambient measurements are not controlled but are $\pm 3^{\circ}$C.

Burning rates at pressures from 34.5 to 345 MPa are determined using a closed bomb combustion technique. A Harwood, 144-cm^3, jacketed powder bomb was used for the closed bomb testing described in this paper. The vessel end closures are equipped with the igniter leads, pressure gauge and vent valves. The inside of the bomb is fitted with a stainless steel liner to protect the inner surface of the chamber body from hostile products and high heating rates of the experiment. The inner chamber with liner is 4.83 cm in diameter with a length of 7.62 cm. Ignition is by means of an Mk2 electric squib. Squib, ignition aid, and propellant sample are contained in a silk bag. A schematic of the closed bomb data acquisition system is shown in Fig. 3. Pressure–time data are acquired using a Kistler model 607C4 pressure transducer. The amplified pressure signal is digitized and recorded using the CBRED[9] closed bomb reduction technique. The program includes the use of variable thermochemistry and a sophisticated treatment of heat losses, ignition, and flame spreading within the sample. Triplicate closed bomb firings at each of two loading densities were used to generate the HMX burning rate curve for pressure above 34.5 MPa. Test-to-test reproducibility was better than 3% for these firings.

Results

Individual regression rate data points for the six monopropellants are summarized in Table 2.

AP

AP samples used for this study included large high-purity single crystals, as well as pressed pellets. The AP single crystals were cleaved to approximately 1 cm $\times$ 0.5 cm $\times$ 0.2 mm size samples. Pellets from various powder lots of AP were pressed. The pellets were pressed at internal die pressures of 335 MPa with a dwell time of 30 min. The resulting pellets had densities of 99.2–99.4% Theoretical Maximum Density (TMD). There was no difference in burning rates between the pressed pellets and single crystals as long as high-purity AP was used in the pellets. Only data for ultrapure AP are presented.

Figure 4 shows the regression rate data for AP at ambient initial temperature. The low-pressure deflagration limit for pure AP at ambient initial temperature is approximately 2 MPa. The negative

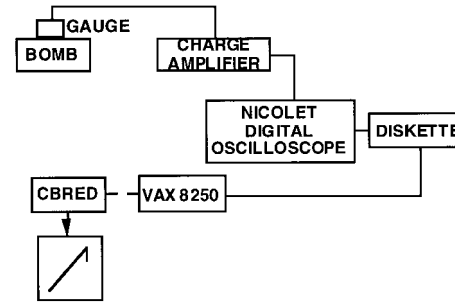

Fig. 3 Schematic of closed bomb data acquisition system.

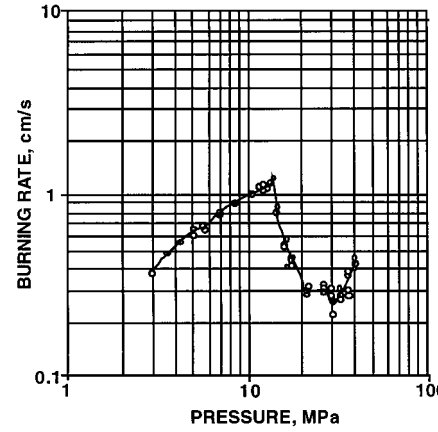

Fig. 4 Burning rate data for ultra-high-purity AP, ambient initial temperature.

Table 2 Individual regression rates

Pressure, MPa (psia)	*R* (meas), cm/s
AP, 298 K	
2.76 (400)	0.381
2.85 (413.8)	0.378
3.54 (513.8)	0.488
4.14 (600)	0.584
4.23 (613.8)	0.564
5.52 (800)	0.737
5.61 (813.8)	0.693, 0.668
6.99 (1,013.8)	0.785, 0.821, 0.815, 0.830
8.27 (1,200)	0.965
8.37 (1,213.8)	0.922, 0.907
10.34 (1,500)	1.067
10.44 (1,513.8)	1.011
11.72 (1,700)	1.128, 1.085, 1.011
12.41 (1,800)	1.130, 1.105, 1.107
13.10 (1,900)	1.163, 1.156, 1.181
13.79 (2,000)	1.237, 1.245
14.48 (2,100)	0.858, 0.813
15.51 (2,250)	0.594, 0.665
15.86 (2,300)	0.518, 0.528
16.38 (2,375)	0.579, 0.406
17.24 (2,500)	0.434, 0.450, 0.432, 0.419
21.37 (3,100)	0.300, 0.315, 0.282, 0.284
26.20 (3,800)	0.312, 0.292, 0.290, 0.302
28.96 (4,200)	0.305, 0.220, 0.274, 0.264
32.20 (4,670)	0.264, 0.262, 0.302, 0.282
35.85 (5,200)	0.388, 0.373, 0.297
38.61 (5,600)	0.445, 0.419, 0.452, 0.396
AP, 323 K	
2.76 (400)	0.406
4.14 (600)	0.584
5.52 (800)	0.737
8.27 (1,200)	0.965
10.34 (1,500)	1.092
AP, 373 K	
2.16 (313.8)	0.356
2.76 (400)	0.457
2.85 (413.8)	0.419, 0.455
4.23 (613.8)	0.640, 0.638.0.566
5.61 (813.8)	0.716, 0.841
6.21 (900)	0.864
6.30 (913.8)	0.864
6.99 (1,013.8)	0.869, 0.864
8.27 (1,200)	1.041
8.37 (1,213.8)	1.016, 1.044
10.34 (1,500)	1.245
10.44 (1,513.8)	1.250, 1.168, 1.146
AP, 423 K	
2.76 (400)	0.508
2.85 (413.8)	0.467, 0.513
4.14 (600)	0.712
4.23 (613.8)	0.701, 0.686
5.61 (813.8)	0.867
6.21 (900)	0.965
6.30 (913.8)	0.956
6.99 (1,013.8)	1.064
8.27 (1,200)	1.041
8.37 (1,213.8)	1.173, 1.255, 1.176
10.34 (1,500)	1.245
10.44 (1,513.8)	1.402, 1.356, 1.562
ADN, 298 K	
0.69 (100)	1.986, 2.174
1.38 (200)	2.517, 2.586
2.76 (400)	3.249, 3.327
3.45 (500)	2.796, 2.116
4.14 (600)	2.669
5.52 (800)	2.487, 3.995
6.90 (1,000)	3.429, 4.882, 2.647, 3.190, 3.579, 2.982
10.34 (1,500)	3.531, 3.691
ADN, 348 K	
0.69 (100)	3.312, 2.126, 2.324
1.38 (200)	3.211, 3.233
2.76 (400)	4.702, 2.985
4.14 (600)	4.003, 3.688
5.52 (800)	3.424, 3.302
6.90 (1,000)	4.265, 3.640
10.34 (1,500)	3.609
RDX, 298 K	
0.69 (100)	0.188, 0.185
1.38 (200)	0.333, 0.320
2.76 (400)	0.564, 0.574
4.14 (600)	0.790, 0.800
5.52 (800)	1.006, 0.996
6.90 (1,000)	1.219, 1.166
10.34 (1,500)	1.646, 1.689
RDX, 373 K	
0.69 (100)	0.211, 0.206
1.38 (200)	0.351, 0.361
2.76 (400)	0.627, 0.607
4.14 (600)	0.876, 0.876
5.52 (800)	1.059, 1.110
6.90 (1,000)	1.349, 1.336
10.34 (1,500)	1.895, 1.895
RDX, 223 K	
0.69 (100)	0.165, 0.180
1.38 (200)	0.302, 0.305
2.76 (400)	0.533, 0.541
4.14 (600)	0.775, 0.749
5.52 (800)	0.955, 0.969
RDX, 423 K	
0.69 (100)	0.274, 0.272
1.38 (200)	0.434, 0.406
HMX, 173 K	
2.07 (300)	0.368, 0.338
2.76 (400)	0.487, 0.437
3.45 (500)	0.531, 0.563
4.14 (600)	0.706, 0.668, 0.630
4.83 (700)	0.724
5.52 (800)	0.737, 0.683, 0.767
6.21 (900)	0.853
HMX, 198 K	
1.38 (200)	0.262, 0.246
1.72 (250)	0.31
2.07 (300)	0.363, 0.353
2.76 (400)	0.495, 0.485, 0.467
3.45 (500)	0.533, 0.549
4.14 (600)	0.650, 0.686
4.83 (700)	0.742, 0.749
5.52 (800)	0.749, 0.848
5.79 (840)	0.874
HMX, 223 K	
1.38 (200)	0.282, 0.227
1.86 (270)	0.33
2.03 (295)	0.351
2.07 (300)	0.348
2.76 (400)	0.459
3.10 (450)	0.523
3.45 (500)	0.551, 0.546
4.03 (585)	0.685
4.14 (600)	0.65
4.83 (700)	0.752, 0.808
5.52 (800)	0.996, 0.800, 0.853, 0.838
6.21 (900)	0.937, 0.968
HMX, 248 K	
0.52 (75)	0.123
0.69 (100)	0.144
0.97 (140)	0.185
1.03 (150)	0.206
1.38 (200)	0.305, 0.277
2.07 (300)	0.381, 0.371
2.76 (400)	0.467
3.45 (500)	0.546, 0.579
4.14 (600)	0.732
4.83 (700)	0.798
5.52 (800)	0.803, 0.698, 0.960, 0.848, 0.874
6.21 (900)	0.96

(Continued)

Table 2 Individual regression rates (continued)

Pressure, MPa (psia)	R (meas), cm/s	Pressure, MPa (psia)	R (meas), cm/s
HMX, 273 K		*HMX, 423 K*	
0.52 (75)	0.117	0.79 (114)	0.389
0.69 (100)	0.136, 0.169	2.14 (310)	0.592, 0.620
0.90 (130)	0.176	5.34 (774)	1.026
1.03 (150)	0.216, 0.225	5.61 (813)	1.064
1.38 (200)	0.283, 0.312, 0.384, 0.295, 0.282	6.94 (1,007)	1.275, 1.307
2.07 (300)	0.368, 0.368, 0.411	10.34 (1,500)	1.750, 1.783
2.76 (400)	0.521, 0.513	*CL-20, 298 K*	
3.45 (500)	0.599	0.69 (100)	0.368, 0.394, 0.582
4.14 (600)	0.63	1.38 (200)	0.597, 0.587, 0.681
4.55 (660)	0.765	2.76 (400)	0.968, 1.123, 1.034
4.83 (700)	0.864	4.14 (600)	1.468, 1.367
5.45 (790)	0.927	5.52 (800)	1.745, 2.144, 1.842
5.52 (800)	0.806, 0.843	6.90 (1,000)	2.347, 2.405, 2.228
6.00 (870)	1.097	10.34 (1,500)	3.023, 3.414, 2.952, 2.875
6.21 (900)	0.998	*CL-20, 373 K*	
HMX, 298 K		0.69 (100)	0.470, 0.551, 0.691
0.24 (35)	0.0955	1.38 (200)	0.693, 0.739, 0.691
0.34 (50)	0.1011	2.76 (400)	1.420, 1.237, 1.252
0.52 (75)	0.1524	4.14 (600)	1.555, 1.509, 1.544
0.69 (100)	0.1626, 0.1669, 0.1694	5.52 (800)	1.880, 1.956, 2.162
1.03 (150)	0.2921, 0.2459	6.90 (1,000)	2.1533, 2.28, 2.284
1.38 (200)	0.2616, 0.3404, 0.2921	10.34 (1,500)	3.198, 3.660, 2.626
2.07 (300)	0.4445	*CL-20, 223 K*	
2.76 (400)	0.5994, 0.5461	0.69 (100)	0.389, 0.340
2.82 (409)	0.536	1.38 (200)	0.561, 0.556
3.45 (500)	0.655	2.76 (400)	0.861, 0.960
4.14 (600)	0.790, 0.686, 0.734	4.14 (600)	1.293, 1.323
4.83 (700)	0.8357	5.52 (800)	1.717, 1.649
4.87 (706)	0.841	*HNF, 298 K*	
5.52 (800)	0.978, 0.965, 0.917	0.69 (100)	0.411, 0.513
6.21 (900)	1.143, 1.034	1.38 (200)	0.841, 0.892
6.98 (1,013)	1.0921, 1.1335	2.76 (400)	1.389, 1.595
10.34 (1,500)	1.4895, 1.6759	4.14 (600)	2.004, 1.991
13.79 (2,000)	3.048	5.52 (800)	2.342, 2.832
20.69 (3,000)	3.302, 3.3378, 4.7244	6.90 (1,000)	2.969, 2.980
27.58 (4,000)	4.318, 4.4958, 5.2578	10.34 (1,500)	4.183
34.48 (5,000)	5.08, 5.334, 6.6548	*HNF, 223 K*	
41.37 (6,000)	6.452	0.69 (100)	0.414, 0.386, 0.391
55.16 (8,000)	8.001	1.38 (200)	0.798, 0.716
68.95 (10,000)	9.144	2.76 (400)	1.255, 1.427, 1.641
137.90 (20,000)	16.256	4.14 (600)	1.755, 1.801
206.85 (30,000)	22.86	5.52 (800)	2.187, 2.667
275.80 (40,000)	31.75	*HNF, 348 K*	
344.75 (50,000)	36.322	0.69 (100)	0.513, 0.523
HMX, 373 K		1.38 (200)	0.932, 0.950
0.79 (114)	0.264	2.76 (400)	1.681
2.14 (310)	0.417, 0.542	4.14 (600)	2.182, 2.20
3.50 (507)	0.725	5.52 (800)	2.761, 2.807
5.57 (808)	1.007, 1.026	6.90 (1,000)	3.2, 3.348
6.94 (1,007)	1.1765	10.34 (1,500)	4.348, 4.780
8.40 (1,218)	1.4085, 1.4802		
10.34 (1,500)	1.625, 1.707		

slope of the burning rate curve between 13.79 and 27.58 MPa is due to unstable combustion, which is further described in Ref. 10. Values of burning rate obtained in the unstable pressure regime are very dependent on the data reduction method. Above 27.58 MPa, combustion becomes more stable with the dominance of gas-phase reactions and the burning rate curve takes on a high positive pressure exponent. The data from Fig. 4 may be compared to that of other investigators in Fig. 5.[10–13]

The burning rate region above 27.58 MPa with its high positive burning rate pressure exponent is of particular interest to the propellant formulator. Considerable increases in propellant performance are possible if the operating pressure of the solid rocket motor were to be increased to pressures greater than 14 MPa. Increased motor operating pressures are possible with current motor case technology. Unfortunately, the high slope region of the neat AP burning rate curve appears to be a limiting factor in achieving the goal of high-pressure burning rates with a low burning rate pressure exponent. Figure 6 illustrates this problem, where the neat AP burning rate curve is represented by the shaded area of the graph. The data

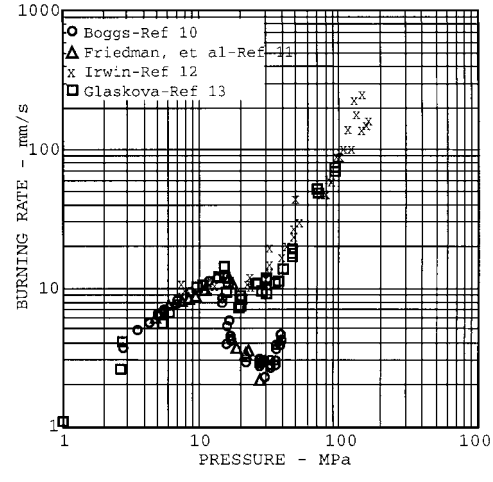

Fig. 5 Comparison of AP burning rate data from various investigators.

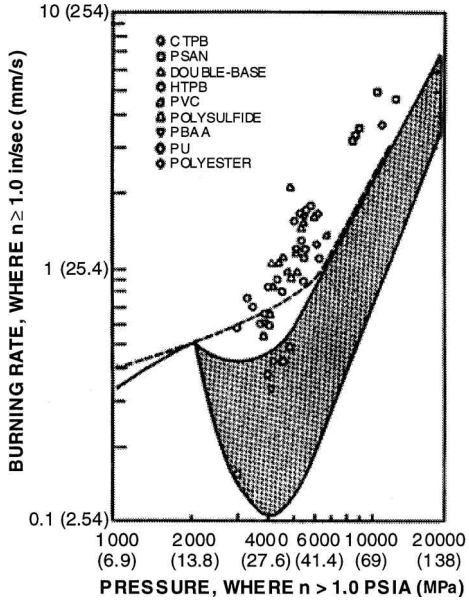

Fig. 6 Effect of neat AP burning rate on burning rate pressure exponent at high pressure.

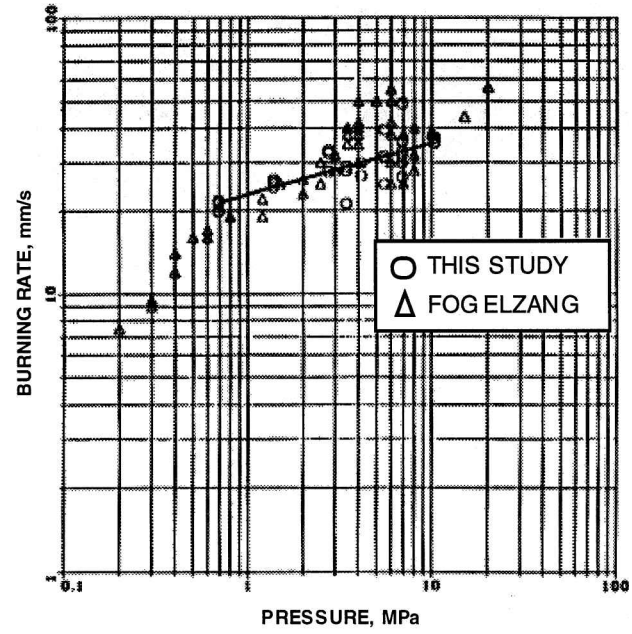

Fig. 8 Comparison of ambient temperature ADN burn data.

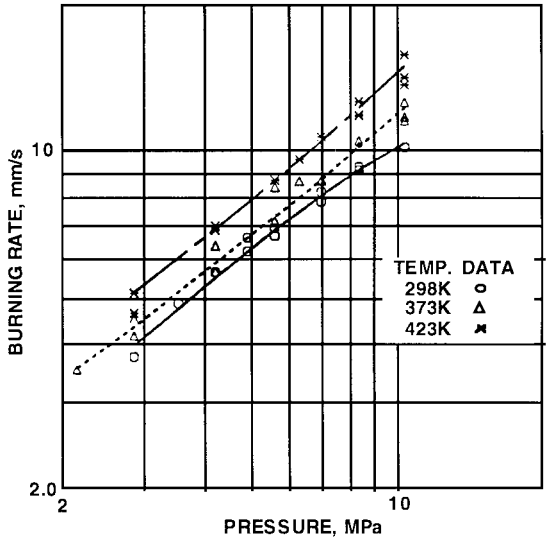

Fig. 7 Temperature and pressure sensitivity of neat AP regression rate.

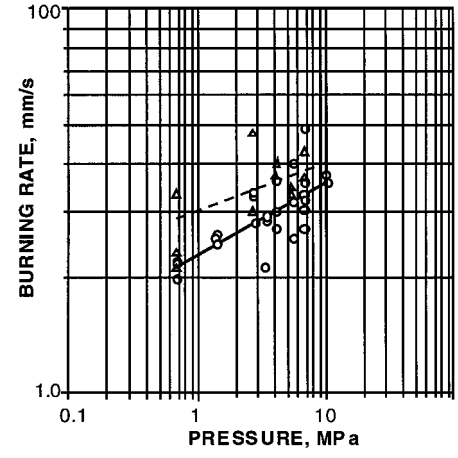

Fig. 9 ADN self-deflagration at two initial temperatures (298 and 348 K).

points represent the pressure where the burning rate pressure exponent is greater than or equal to unity for a number of AP-based propellant systems of various binder types. It can be seen that for low burning rate propellants the transition to high burning rate exponent occurs at lower pressures that those with higher burning rates; however, all of the data are located to the left of the high slope neat AP burning rate regime. The authors would be very interested in obtaining AP-based propellant burning rate data that contradict this observation.

The AP self-deflagration data at three initial temperatures (298, 373, and 423 K) over the pressure range of 2.16–10.3 MPa are presented in Fig. 7. Note that the spacing between the burning rate curves is not uniform. The increase in burning rate and, thus, temperature sensitivity, becomes greater with increasing temperature.

ADN

ADN powder was dry pressed at 621 MPa and held for 10 min. The resulting rectangular pellets were 97–98% TMD. The sample sources of ADN consisted of small batches synthesized at the U.S. Naval Air Warfare Center Weapons Division (NAWCWD) by Hollins and also a sample from SRI International. Because of the low melting point of this material (365–367 K), it is impossible to test this material at conditions similar to the other materials.

The ADN burning rates at ambient temperature are quite high, with relatively low burning rate pressure exponent; however, the data displayed considerable scatter in the pressures between 2 and 10 MPa. The ambient ADN data are compared to those of Fogelzang et al.[14] in Fig. 8, where the data scatter is also observed. Fogelzang et al. attribute this data scatter to unstable combustion, but it may be also due to the deconsolidation of the material due to thermal stresses in the crystalline sample. Thermal deconsolidation has been observed with large unconfined single crystals of HMX. Deflagration measurements were only possible when the crystals were rigidly confined with an epoxy.[15] Further combustion work on rigidly confined ADN single crystals, as well as well compacted powder, is needed to resolve this issue.

ADN burning rate data at two initial temperatures (298 and 348 K) over the pressure range of 0.69–10.3 MPa are presented in Fig. 9.

HMX

The HMX ambient temperature burning rate results from 0.24 to 345 MPa are plotted in Fig. 10. All three experimental techniques described earlier were used to obtain the burning rate data over

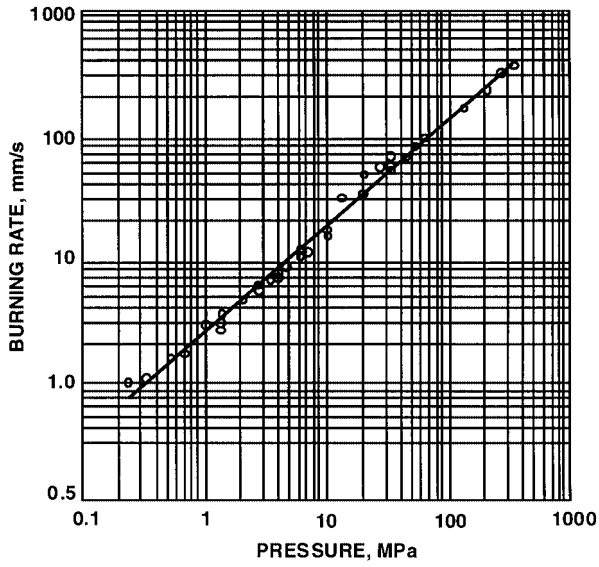

Fig. 10 Ambient temperature HMX burning rate data.

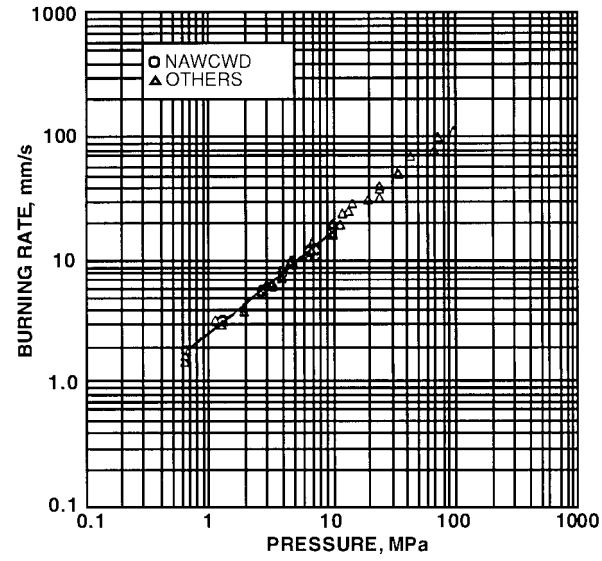

Fig. 12 RDX burning rate data at ambient initial temperature.

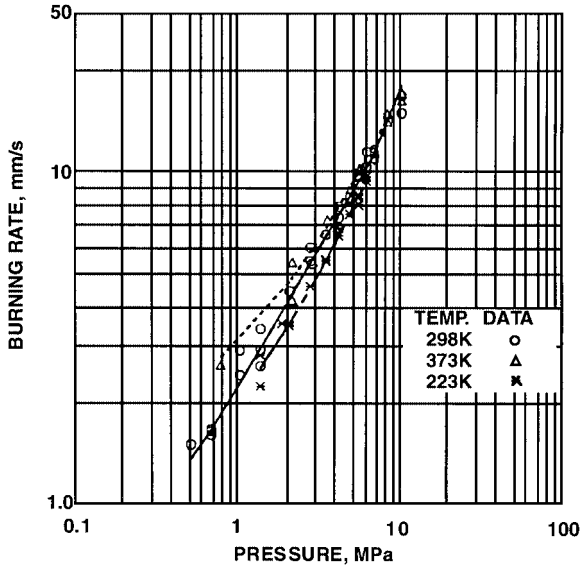

Fig. 11 HMX self-deflagration at three initial temperatures.

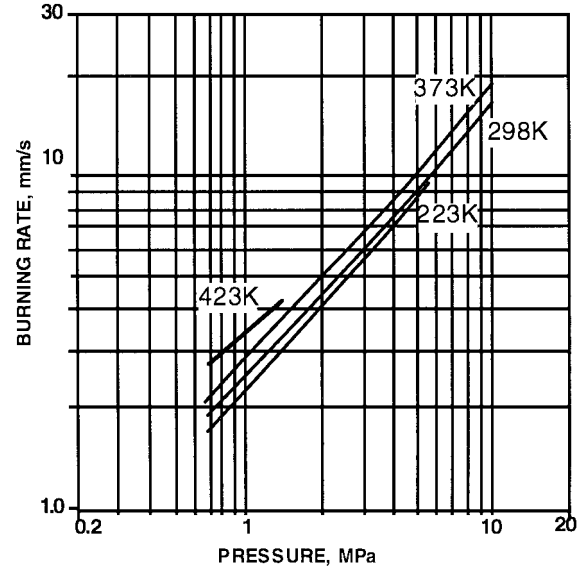

Fig. 13 RDX self-deflagration data from 0.69 to 10.3 MPa at four initial temperatures (223, 298, 373, and 423 K).

such a broad range of pressures. Additionally, samples consisted of large high-purity single crystals and pressed pellets for the lower pressure work and a carefully screened powder of uniform particle size that was burned in the high pressure closed bomb. Figure 10 demonstrates the ability to successfully merge the data of different experiments and sample types and should provide a good test of analytical models to predict the burning rates over a broad range of pressures.

The HMX self-deflagration data at three initial temperatures (223, 298, and 373 K) over the pressure range of 0.5–10.3 MPa are presented in Fig. 11. The burning rate data at additional temperatures may be found in Table 2. As the pressure increases, the effect of initial temperature is decreased.

RDX

RDX powder was pressed into rectangular pellets using 20 μl of acetone per 0.5 g pellet as a bonding agent. The pellets were pressed at 621 MPa and held for 5 min. The resulting pellets were 95.5–99.1% TMD.

In Fig. 12, ambient initial temperature RDX burning rate data from this study are compared to the results of others (personal communication with M. W. Beckstead, who provided data from Zimmer-Galler and Glaskova). Figure 13 presents the pressure and temperature sensitivity for burning rates of pressed pellets of RDX. Only two pressures were evaluated at 423 K initial temperature, 0.69 and 1.38 MPa.

CL-20

Rectangular pellets of CL-20 were solvent pressed at 896 MPa for 10 min with 20 μl of acetone added per 0.5 g of CL-20. The resulting pellets were 94–98% TMD.

Figure 14 presents the CL-20 burning rate temperature and pressure sensitivity data at three initial temperatures (223, 298, and 373 K) at pressures from 0.69 to 10.3 MPa.

HNF

Cylindrical pellets (6.6 mm diam) of HNF were pressed at 6.21 MPa for 5 min. Care had to be taken that pressing was performed in a low-humidity environment as the material appeared to be hygroscopic. The resulting pellets were 93–95% TMD. Like ADN, HNF has a low melting point (398 K) restricting the evaluation of burning rate temperature sensitivity.

The ambient temperature burning rates are compared to data from Atlantic Research Corporation (ARC)[16] and TNO Prins Maurits Laboratory in Figs. 15 and 16. The ARC burning rate data were

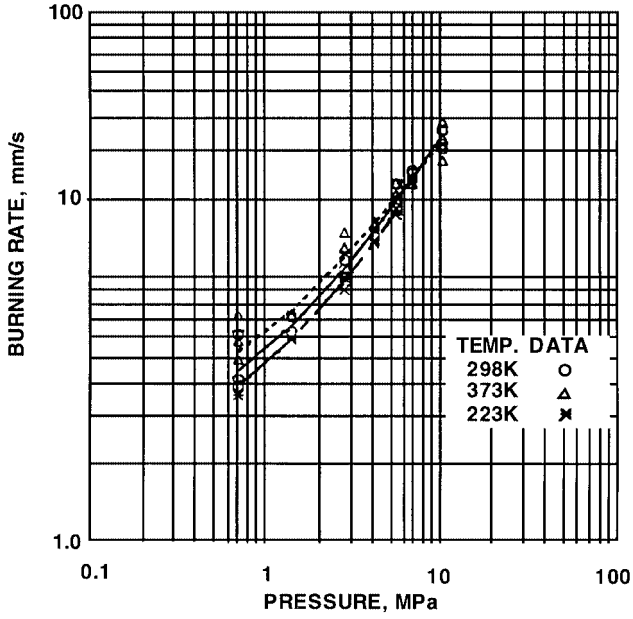

Fig. 14 CL-20 burning rate data at three initial temperatures.

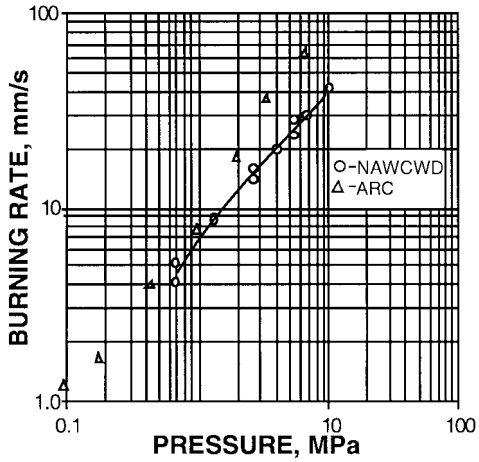

Fig. 15 Comparison of HNF burning rate data from ARC and NAWCWD data.

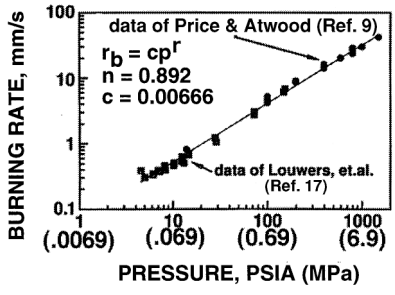

Fig. 16 Comparison of HNF burning rate data (TNO, Louwers) to NAWCWD.

generated using straws filled with HNF powder, thus the combustion at pressures of 2 MPa and higher may be more representative of convective burning rather than a laminar burn. Elsewhere, the burning rates are comparable.

The HNF burning rate data at three initial temperatures (223, 298, and 348 K) are presented in Fig. 17 for pressures from 0.69 to 10.3 MPa. The ambient temperature burning rates for the various ingredients are compared in Fig. 18.

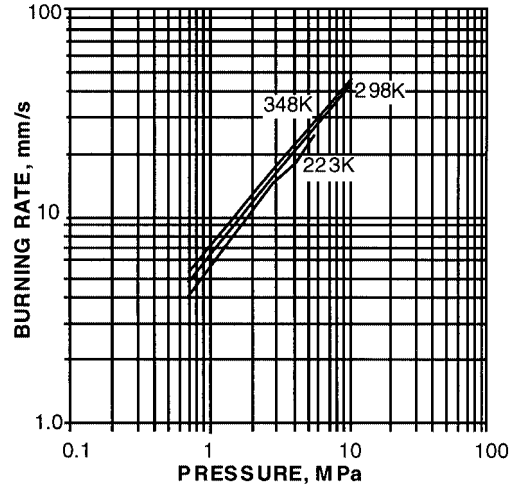

Fig. 17 HNF burning rate data at three initial temperatures (223, 298, and 348 K).

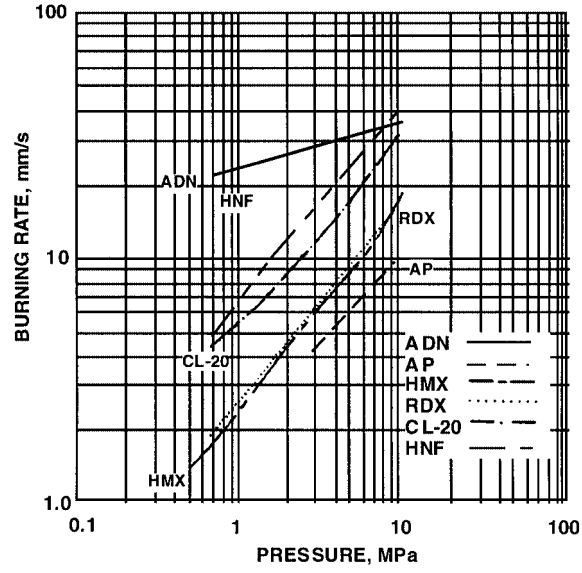

Fig. 18 Self-deflagration at ambient initial temperature of six monopropellants.

Summary

In Fig. 18, it can be seen that ADN and HNF have the highest burning rates of the ingredients tested with AP having the lowest. Of the nitramines, RDX and HMX have comparable burning rates but are a factor of two lower than CL-20. HNF, with the highest burning rate pressure exponent (about 0.89), surpasses ADN in burning rate at pressures above 8 MPa. It appears that due to the low slope of the ADN burning rate curve, the CL-20 burning rates above 14 MPa may exceed those of ADN as well. Further comparisons of the ingredient burning rates will be made in the second paper of this series.

This paper presents the self-deflagration data for a set of six energetic materials that are currently being used as solid rocket motor ingredients. The data were generated under similar conditions to maintain a uniform, self-consistent data set. The data can be used in a number of modeling applications to either verify the prediction of self-deflagration or as input parameters into those models (such as used to predict various hazards) requiring a description of the deflagration process.

References

[1] Novozhilov, B. V., "Theory of Nonsteady Burning and Combustion Stability of Solid Propellants by the ZN Method," Vol. 143, Progress in Astronautics and Aeronautics, AIAA, Washington, DC, 1992, Chap. 15, pp. 601–641.

[2]Sutton, G. P., *Rocket Propulsion Elements An Introduction to the Engineering of Rocket*, 5th ed., Wiley, New York, 1986, p. 361.

[3]Boggs, T. L., Atwood, A. I., Curran, P. O., Parr, T. P., Hanson-Parr, D., and Paull, D., "The Pressure and Temperature Sensitivity of Burning Rates of Solid Propellant Ingredients," *Proceedings of the International Symposium on Energetic Materials*, 1995.

[4]Prasad, K., Smooke, M. D., Tanoff, M., and Yetter, R. A., "Modeling the Deflagration of HMX at High Pressures," *Proceedings of 1996 JANNAF 33rd Combustion Subcommittee Meeting*, Publ. 563, Vol. II, Chemical Propulsion Information Agency, Laurel, MD, 1996, pp. 557–568.

[5]Jing, Q., Jeppson, M., and Beckstead, M. W., "Influence of AP-Solid Phase Decomposition on Temperature Profile and Sensitivity," *Proceedings of 1997 JANNAF 34th Combustion Subcommittee Meeting*, Publ. 662, Vol. IV, Chemical Propulsion Information Agency, Laurel, MD, 1997, pp. 99–108.

[6]Boggs, T. L., Crump, J. E., Kraeutle, K. J., and Zurn, D. E., "Cinephotomicrography and Scanning Electron Microscopy as Used to Study Solid Propellant Combustion," *Experimental Diagnostics in Combustion of Solids*, Vol. 63, Progress in Astronautics and Aeronautics, 1978, AIAA, New York, pp. 20–47.

[7]Price, C. F., and Juhasz, A., "A Versatile User-Oriented Closed Bomb Data Reduction Program (CBRED)," U.S. Army Ballistic Research Lab. Rept. 2018, Aberdeen Proving Ground, MD, Sept. 1977.

[8]Parr, T. P., and Hanson-Parr, D. M., "Measurement of the Temperature Sensitivities of ANAP-A* and HMX Burning Rates," *19th JANNAF Combustion Meeting*, publ. 366, Vol. 1, Chemical Propulsion Information Agency, Laurel, MD, 1982, pp. 281–288.

[9]Price, C. F., and Atwood, A. I., "CBRED II, A Versatile Tool for the Characterization of Damaged Propellants," *Proceedings of the 1991 JANNAF Propulsion Systems Hazards Subcommittee Meeting*, publ. 562, Chemical Propulsion Information Agency, Laurel, MD, 1991, pp. 425–431.

[10]Boggs, T. L., "Deflagration Rate, Surface Structure, and Subsurface Profile of Self-Deflagrating Single Crystals of Ammonium Perchlorate," *AIAA Journal*, Vol. 8, No. 5, 1970, pp. 867–873.

[11]Friedman, R., et al., "Deflagration of Ammonium Perchlorate," *Sixth Symposium (International) on Combustion*, Reinhold, New York, 1957, pp. 612–618.

[12]Irwin, O. R., Salzman, P. K., and Anderson, W. H., "Deflagration Characteristics of Ammonium Perchlorate at High Pressures," *Ninth Symposium (International) on Combustion*, Academic, New York, 1963, pp. 358–364.

[13]Glaskova, A. P., "Effect of Pressure on the Combustion Rate of Ammonium Perchlorate," *Zhurnal Prikladnoi Mekhanika i Teknicheskoi Fiziki*, No. 5, 1963; trans. (DDC AD614 773), pp. 193–202.

[14]Fogelzang, A. E., Sinditskii, V. P., Egorshev, V. Y., Levshenkov, A. I., Serushkin, V. V., and Kolesov, V. I., "Combustion Behavior and Flame Structure of Ammonium Dinitramide," *Combustion and Detonation*, 28th International Annual Conference of ICT, Fraunhofer-Institut für Chemische Technologie, Karlsruhe, Federal Republic of Germany, 1992, pp. 99-1–99-14.

[15]Derr, R. L., Boggs, T. L., Zurn, D. E., and Dibble, E. J., "The Combustion Characteristics of HMX," *11th JANNAF Combustion Meeting*, Publ. 261, Vol. I, Chemical Propulsion Information Agency, Laurel, MD, 1974, pp. 231–241.

[16]McHale, E. T., and von Elbe, G., "The Deflagration of Solid Propellant Oxidizers," *Combustion Science and Technology*, Vol. 2, 1970, pp. 227–237.

[17]Louwers, J., Parr, T., and Hanson-Parr, D., "Decomposition and Flame Structure of Hydrazinium Nitroformate," 37th AIAA Aerospace Sciences Meeting and Exhibit, AIAA Paper 99-1091, Jan. 1999.